Fermilab FERMILAB-Conf-03/209-E December 2003

RECENT RUN II ELECTROWEAK AND QCD RESULTS FROM DØ

Robert Kehoe (*for the DØ Collaboration)*
Michigan State U., Dept. Physics and Astronomy, East Lansing, MI 48824

Abstract

The DØ Detector is a hermetic, multipurpose detector residing at one interaction region designated for $p\overline{p}$ collisions at 2 TeV at the Fermilab Tevatron. Both the detector and accelerator have undergone major upgrades to increase the luminosity and handle higher interaction rates. This paper presents recent results from Run II data which explore QCD and electroweak physics at the energy frontier. The dijet mass cross section and a search for Z' in dielectron decays are presented, and these are already approaching sensitivities seen in Run I. Additionally, the first measurement of the $\sigma_Z * BR(Z \to \mu\mu)$ is given for the new collision energy.

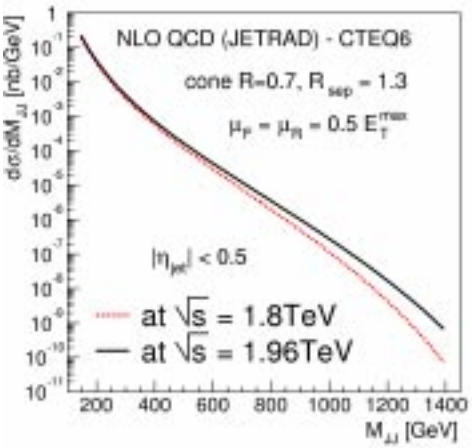

Figure 1: *The calculated NLO cross-section vs dijet invariant mass is shown. The increase in cross section for large masses is indicated.*

1 DØ at the Tevatron

As a multipurpose collider detector, DØ has the typical three main divisions of the type: innermost tracking, calorimetry, and outermost muon tracking. The tracking detectors are completely new for Run II of the Tevatron and consist of a compact silicon vertex detector surrounded by a scintillating fiber tracker. These are, in turn, surrounded by a 2T solenoid permitting momentum measurement of individual tracks. Both the silicon and fiber trackers provide full coverage for particles more central than $|\eta| = 2.0$, and moderate coverage in the forward region. Covering the full region to $|\eta| = 5$, the calorimetry is primarily comprised of the central and endcap cryostats utilizing depleted uranium absorber and liquid argon as the sampling medium. Much of the electronics for the calorimeter have been replaced to handle the higher collision rates in Run II. The central muon system consists of one layer of proportional drift tubes before and two layers after a 1.4 T toroid and covers the region $|\eta| < 1.0$. The new forward system covers to $|\eta| = 2.0$ and is composed of mini-drift tubes.

The trigger is three-tiered consisting of one hardware followed by two consecutive software levels. This system is currently reading out to tape at the 50 Hz design goal. Data-taking efficiency is currently approximately 85% and improving.

2 Dijet Mass Cross Section

QCD next-to-leading order (NLO) calculations can be probed via measurement of the cross section of dijets vs. the dijet invariant mass. For instance, QCD

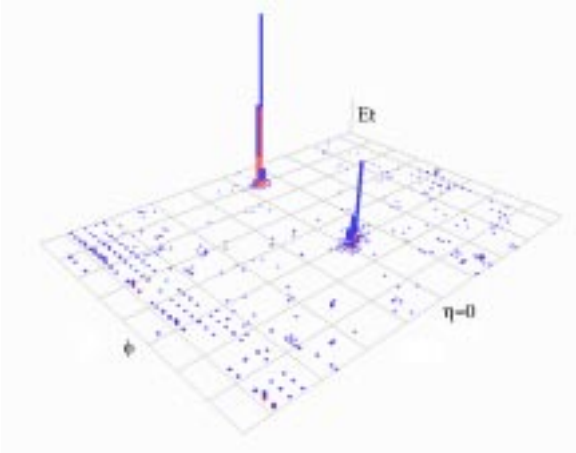

Figure 2: *Highest mass event with two leading jets in central ($|\eta| \leq 0.5$) region. The mass is 838 GeV.*

predicts a factor of two increase in cross section at high mass when comparing $\sqrt{s} = 1.8$ and 2 TeV (see Figure 1). On an absolute scale, we really test QCD folded with parton distribution functions (PDFs) and a measure of the high mass cross section provides a handle on the proton structure at large values of x. The identification of a resonance at high mass would indicate new physics. Quark compositeness would show up as an increased cross section at very high mass scales.

The data sample used for this analysis is 34.1 pb^{-1}. For event quality, we require that the missing transverse energy, $\not\!\!E_T$, satisfy the relation $\frac{\not\!\!E_T}{P_T^{j1}} < 0.7$. This removes rare instrumental backgrounds to high E_T jet events. We also require that the primary vertex be reconstructed with at least 4 tracks, and that $|z| < 50$ cm. Jets are reconstructed using the Run II cone algorithm as defined in [1]. The jets are required to satisfy $|\eta| \leq 0.5$ and at least two jets are required. The invariant mass is calculated from the leading two jets. Under these conditions the highest mass observed with two central leading jets is 838 GeV, shown in Figure 2.

2.1 Jet Energy Scale

The measured raw momentum of jets is ideally the vector sum of the momenta of the constituent particles. However, even aside from the inherent energy resolution of the calorimeter, a number of effects degrade the one-to-one correspondence between input particle momenta and observed jet energy.

First, there is an *offset* coming mainly from physical underlying event and net energy from asymetric noise after pedestal suppression. This can be measured at low luminosity by taking the typical E_T density in minimum bias

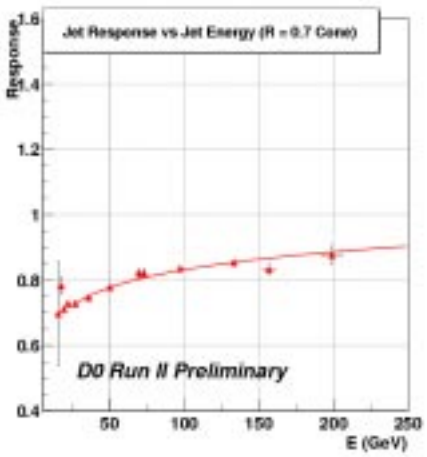

Figure 3: *Jet response vs. jet energy for* $\Delta R = 0.7$ *cone jets. The logarithmic fit vs. energy is indicated.*

events. Second, the detector itself has an energy *response* different from 1.0 due to small but non-negligible nonlinearities and dead regions. We currently utilize the method of measuring this developed in Run I [2] which employs total event E_T imbalance (i.e. $\not\!\!E_T$) in direct photon plus jet candidate events. The response as a function of jet energy is shown in Figure 3. Third, particles shower transversely in the detector sometimes causing them to spill energy outside of their jet cone. We determine this from jet transverse shapes as measured in data.

Errors for the jet energy scale are currently largely statistical, particularly in the central region. However, as the jet energy increases past 200 GeV, the systematic error also increases because we are extrapolating from small photon statistics.

2.2 Trigger Selection

We utilize four triggers for this analysis with Level 3 E_T jet thresholds of: 25 GeV, 45 GeV, 65 GeV and 95 GeV. An offline invariant mass cut is also applied for events from each trigger to ensure full efficiency. These thresholds are: 150 GeV, 180 GeV, 300 GeV and 390 GeV. The mass spectrum and approximate prescales for these triggers are shown in Figure 4. The overlap of the distributions for adjacent triggers indicates the validity for the offline mass cuts.

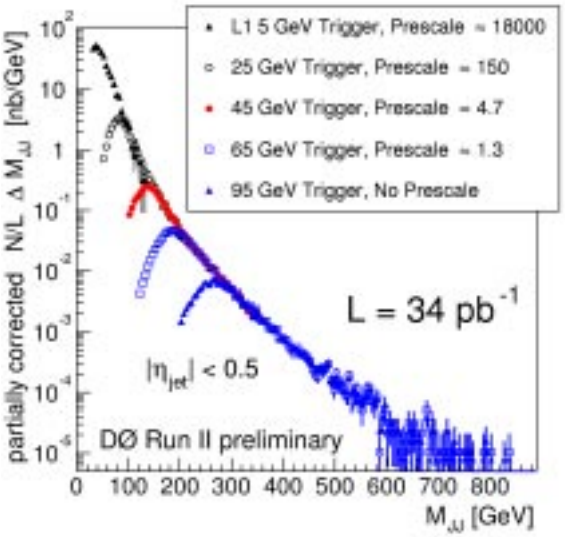

Figure 4: *Invariant mass spectra passing four high E_T inclusive jet triggers plus a low E_T trigger for comparison. Effective prescales and Level 3 E_T thresholds are indicated.*

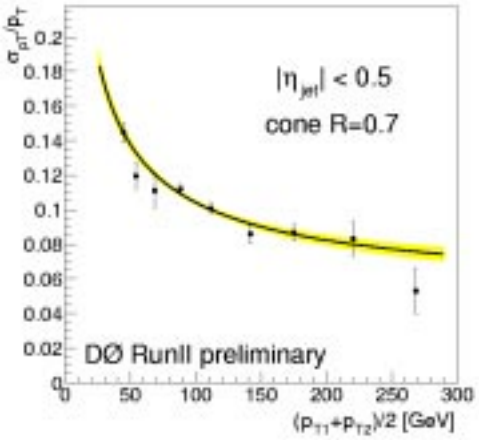

Figure 5: *Fractional E_T resolutions as a function of typical E_T for central jets with a cone of $\Delta R = 0.7$. Uncertainties are statistical only.*

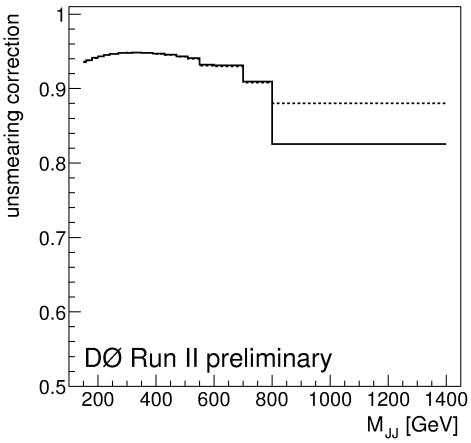

Figure 6: *Bin-by-bin unsmearing correction vs. dijet mass. Both ansatz functions shown are in agreement.*

2.3 Energy Resolution

Given a fundamentally falling cross section with increasing mass, the jet resolutions modify the observed histogram of events vs. mass. This effect must be unfolded in order to quantify the underlying cross section behavior. The first step of this correction involves the determination of the jet energy resolution itself. We use essentially the same sample of dijet events as the invariant mass cross section analysis. We calculate in each event an asymmetry parameter,

$$A = \frac{P_T^{jet1} - P_T^{jet2}}{P_T^{jet1} + P_T^{jet2}} \tag{1}$$

which is related to the fractional energy resolution by $\frac{\sigma_{P_T}}{P_T} = \sqrt{2}\sigma_A$. This resolution can then be plotted vs. the average jet energy in the event as shown in Figure 5. We further correct this value for unfound third jets and for the effect of particle jet resolution which should not be included in the unsmearing.

We consider two different ansatz functions which describe the functional form of the fundamental 'true' cross section with mass. These functions are then smeared and a χ^2 is calculated with respect to the data. The function parameters are tuned by minimizing this χ^2. The ratio of the final ansatz function to the final smeared distribution provides the unsmearing correction. Figure 6 shows the result of this fit in each mass bin. The correction is essentially flat as a function of mass, and the two ansatz functions give essentially the same unsmearing correction.

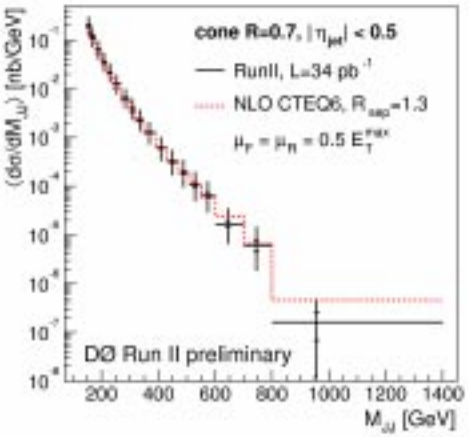

Figure 7: *Cross section vs. M_{jj}. NLO QCD (dotted histogram) agrees with observation within uncertainties.*

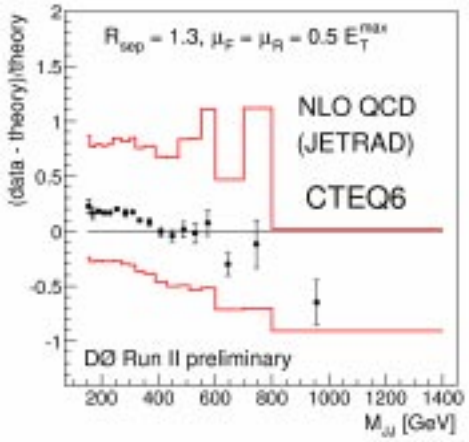

Figure 8: *(data-theory)/theory using CTEQ6 pdf. Total uncertainty indicated (solid band).*

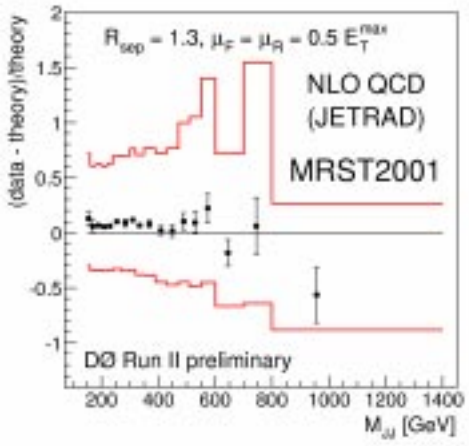

Figure 9: *(data-theory)/theory using MRST2001 pdf. Total uncertainty indicated (solid band).*

2.4 Observed Cross Section

The observed cross section can be calculated by

$$\left\langle \frac{d\sigma}{dM_{jj}} \right\rangle = \frac{N_{evt}}{L\epsilon_{eff}} \frac{C_{unsmear}}{\Delta M_{jj}} \tag{2}$$

where ϵ_{eff} quantifies cut efficiences and $C_{unsmear}$ is the unsmearing correction per mass bin. Cut efficiencies are estimated from data to be 78% for vertex quality, and 97% for jet quality. The cross section vs. invariant mass is indicated in Figure 7 with the total error. The 10% luminosity error, which is fully correlated bin-to-bin, is not shown. Within errors, there is agreement with the NLO theory using the CTEQ6 pdf.

In order to see the level of agreement, we plot (data-theory)/theory using CTEQ6 (Figure 8) and MRST2001 (Figure 9). There is agreement within the rather large uncertainties. The E_T resolution and jet quality uncertainties are sizable, but the overall uncertainty is dominated by the jet energy scale uncertainty. The jet energy scale uncertainty is $\pm^{52\%}_{38\%}$ for the 150 GeV to 160 GeV bin, and $\pm^{190\%}_{73\%}$ for the 800 to 1400 GeV bin.

3 Measurement of $\sigma_Z * BR(Z \to \mu\mu)$

One of the key measurements of DØ's electroweak physics program concerns the measurement of the production cross sections of the W and Z vector bosons. We have previously presented preliminary measurements of $\sigma * BR$ for the electron decays of these states; here we present the first $Z \to \mu\mu$ measurement from Run II.

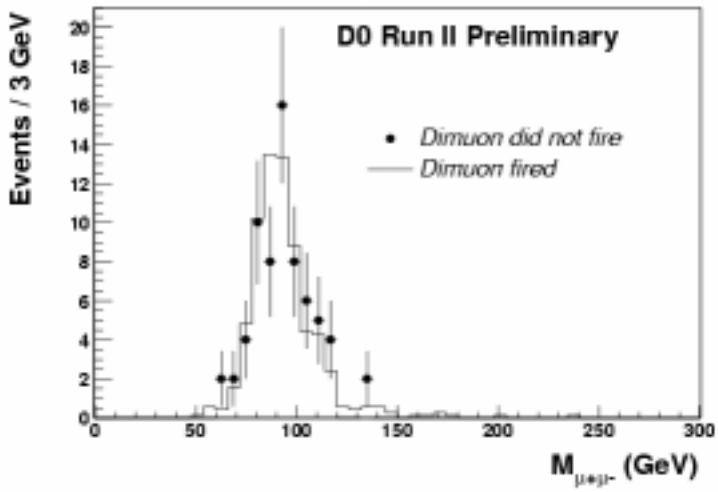

Figure 10: *$M_{\mu\mu}$ for dimuon events when probe muon fired Level 1 (histogram) and did not fire Level 1 (points). Similar shpaes indicate low background in efficiency determination.*

We employ a trigger which requires two muons at Level 1, and one muon at Level 2. For this analysis, we gathered 31.8 pb^{-1} of the data taken with this trigger. The trigger efficiency is measured from data. For instance, the Level 1 single muon efficiency is obtained by considering a *tag* muon from the Z and matching it to a fired Level 1 muon in a single muon trigger. The low background under the Z means that we can estimate the Level 1 muon efficiency for the other *probe* muon by counting the rate at which the dimuon trigger fires in this sample (see Figure 10). The Level 1 efficiency is 91%. A similar approach is taken for Level 2 and gives a single muon efficiency of 86%. These efficiencies have since been improved.

Our offline event selection requires two muons, each within $|\eta| < 1.8$, and each matching a track in the fiber and silicon trackers. The tracking efficiency is estimated using the same tag/probe approach as described above, where here the probe muon may lack a track match. The calculated tracking efficiency is currently 82%. This inefficiency is considerably reduced in more recent versions of the reconstruction as the tracking algorithms are optimized. Each muon must have $P_T > 15$ GeV and must be isolated in both the calorimeter and the tracker. Timing cuts are employed to remove the low cosmic ray background. The muons must be oppositely charged and have a separation in $\eta - \phi$ of $\Delta R_{\mu\mu} > 2.0$. 1585 events pass these cuts.

3.1 Dimuon Backgrounds

The Z dimuon background consists of three components: heavy flavor (i.e. $b\bar{b}$), $Z \to \tau\tau$, and Drell-Yan. Heavy flavor production can result in occasional

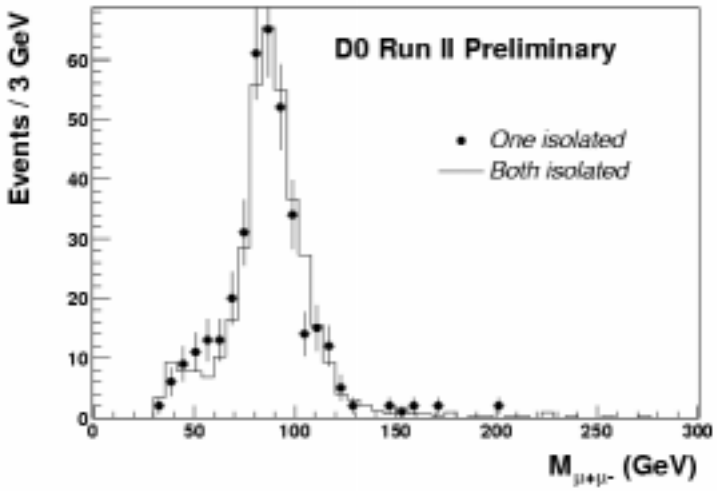

Figure 11: *$M_{\mu\mu}$ for dimuon events when probe muon is isolated (histogram) and not isolated (points). Similarity indicates heavy flavor (i.e. non-isolated) muon background is small and estimated to be $1\% \pm 1\%$ of sample with only one isolated muon.*

events where two muons from b or c decay appear isolated. We consider the high P_T dimuon sample and observe the change in shape of the invariant mass distribution when we remove the isolation requirement on one of the muons. The heavy flavor contribution would preferentially congregate at low masses (i.e. just above the kinematically required 30 GeV). As shown in Figure 11, we observe no difference between the sample with one isolated muon and two isolated muons. Given the statistics, this background is less than 1%. Therefore, we assume this background is 1% of the total dimuon sample and consider this estimate as having a 1% systematic uncertainty.

In order to understand the $Z \to \tau\tau \to \mu\mu$ and the Drell-Yan background, we utilize PYTHIA and a fast detector simulation. The muon resolution has been tuned to that measured in data. The $Z \to \tau\tau$ background is shown in Figure 12 and is $< 1\%$ of the high P_T dimuon sample. The Drell-Yan background is estimated by comparing a sample of Z dimuon events with a sample of $Z + \gamma^*$ dimuon events. A correction factor is derived ($= N_Z / N_{Z+\gamma^*}$) which allows us to account for the number of γ^* events we should observe.

3.2 Measured $\sigma * BR$

The efficiency calculation for this analysis can be factored as

$$\epsilon_Z = \epsilon_{MC}^{eff} \times \epsilon_{fz} \times (2\epsilon_{L2} - \epsilon_{L2}^2) \times \epsilon_q \times \epsilon_{isol} \times \epsilon_{cosmic} \qquad (3)$$

where the last three terms concern opposite charge, isolation and cosmic veto requirements for muons. The first term, ϵ_{MC}^{eff}, contains several components

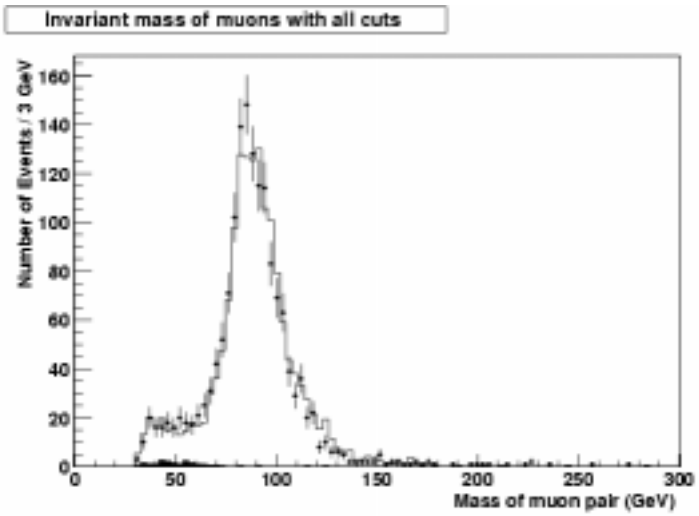

Figure 12: *$M_{\mu\mu}$ for dimuon events for Z+Drell-Yan Monte Carlo (histogram), $Z \to \tau\tau$ (solid, near 50 GeV masses) and data (points). The Z+Drell-Yan provides a good description of the observed distribution.*

containing the main inefficiency and uncertainty contributions for the cross section determination. The components of this term are the raw acceptance from Monte Carlo (0.403 ± 0.012), Level 1 muon (0.912 ± 0.017), loose muon identification (0.909 ± 0.01) and track efficiency (0.822 ± 0.014). Our determination is

$$\sigma * BR = 263.8 \pm 6.6(stat) \pm 17.3(sys) \pm 26.4(lum)\, pb.$$

Figure 13 indicates this measurement in addition to other measurements of the W and Z cross sections at hadron colliders.

4 $Z' \to ee$ Search

The existence of a neutral vector boson similar to the Z but heavier is expected in many models which describe new physics. One popular variation on these consists of the so called left-right symmetric models which postulate a right-handed gauge group $SU(2)_R$ to restore parity symmetry. Such a theory has the added feature that small masses for left-handed neutrinos are naturally accounted for.

In general, a search for a Z' as predicted by the various models and decaying to dielectrons naturally shares a lot with analyses studying dielectron decays of the Z boson. Our search pursues this path with an emphasis on maximizing efficiency. The data sample used for this analysis consists of 50 pb^{-1} of collider data. A single electron trigger is used which requires one Level 1 electromagnetic tower and a Level 3 electron with shower shape cut.

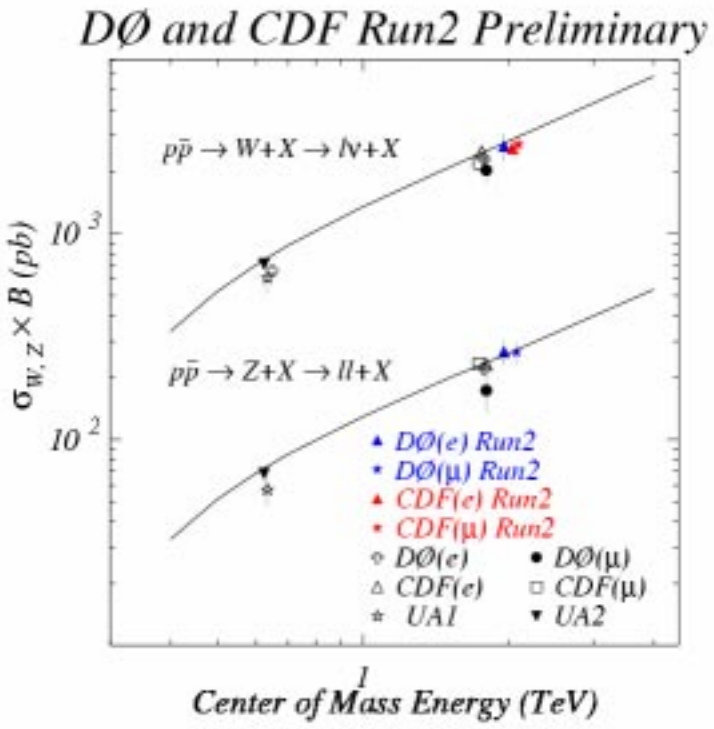

Figure 13: $\sigma_{Z,W}$ *vs. center of mass energy.*

The kinematic selection requires two electron candidates with $|\eta| < 2.5$ and $E_T > 25$ GeV. Electron identification utilizes only calorimeter-based quantities including isolation and energy fraction in electromagnetic layers. We also use an H-matrix shower shape cut. This presents a special challenge because the Z' search probes much higher electron energies than are observed in typical Z decays. Because the shower shape will alter as the electron energy increases, and because the normal shower shape efficiencies are measured from the Z sample, we determined how to effectively use this parameter to select high mass Z's. We generate Z's with PYTHIA in mass bins from 300 GeV thru 800 GeV and process all events with a full plate level GEANT simulation. The efficiency of a fixed cut is observed to fall with energy, so we adopt a E_T-dependent H-matrix cut for this analysis.

4.1 Backgrounds

The background for high mass dielectron events comes from Z+Drell-Yan production and the QCD fake background. To study the former, we generate PYTHIA events using the CTEQ4L pdf in conjunction with the fast detector simulation described earlier. We correct the leading order cross section calculated by PYTHIA with a mass-dependent factor derived from [3].

The QCD instrumental background arises predominantly from dijet events

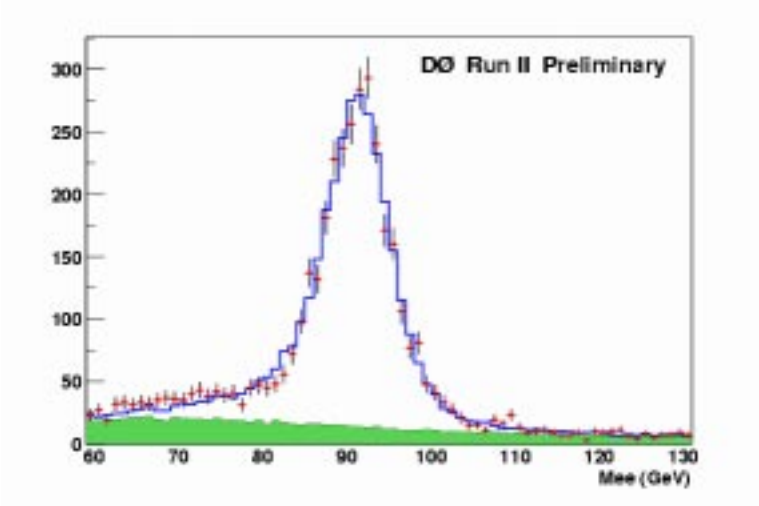

Figure 14: *QCD (green) and Z+Drell-Yan (solid histogram) contributions in the Z mass region.*

where one jet fragments to a leading π°. This background dominates at high mass where the Drell-Yan cross section falls off rapidly. We obtain the M_{ee} distribution for this background from the data.

Once we have the shapes of the Drell-Yan and QCD backgrounds, we determine the normalization for each by allowing each to float in a fit to the dielectron data in the mass window 65 GeV $< M_{ee} <$ 115 GeV. The result is indicated in Figure 14.

4.2 Results

Figure 15 shows the full M_{ee} spectrum. The highest mass event with two central electrons has $M_{ee} = 386$ GeV and is shown in Figure 16. The data points are consistent with the sum of Drell-Yan and QCD for all masses. Figure 15 also indicates an example of a Z' with 600 GeV mass.

The lack of an excess translates into a limit on the cross section for Z' production. In order to relate this cross section limit to a limit on the mass, we consider a reference model with the following properties. We assume the coupling to quarks and leptons is the same as the standard model Z, and that top decays are available when $M_{Z'}$ permits. We also assume that the Z' width scales with mass like the Z, and that decays to Zs are suppressed. For this kind of Z', we can determine, as a function of $M_{Z'}$, the dependence of the acceptance to find two electrons satisfying our selection. We utilize our Z' events calculated with PYTHIA and the fast detector simulation, and calculate the acceptance relative to that of a Z as a function of Z' mass. The increased acceptance with $M_{Z'}$ is plotted in Figure 17.

Given this acceptance and the couplings to quarks, we can determine a

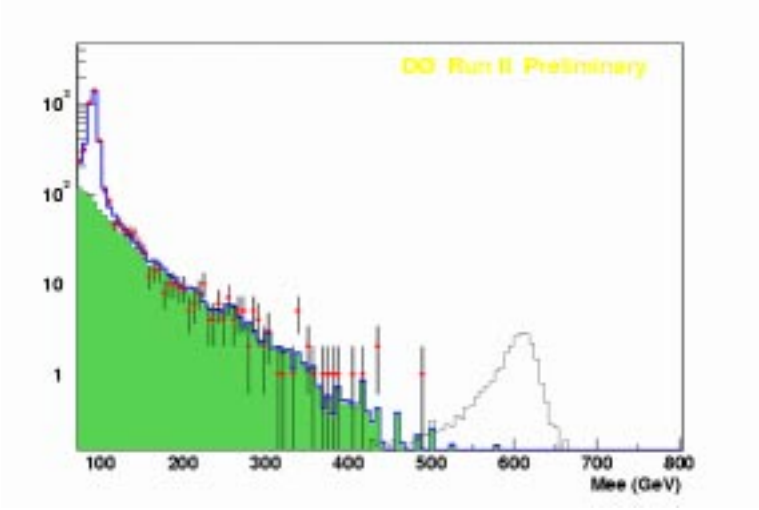

Figure 15: *QCD (green) and Z+Drell-Yan (solid histogram) contributions at all reconstructed masses. The data agree well with the background expected. An example Z′ peak at 10x the expected statistics is shown for comparison.*

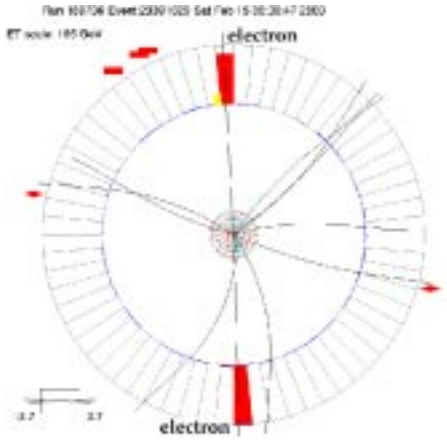

Figure 16: *Highest mass event with two electrons in central region. M_{ee} = 386 GeV. Two electrons in the calorimeter are indicated top and bottom, along with matching central tracks.*

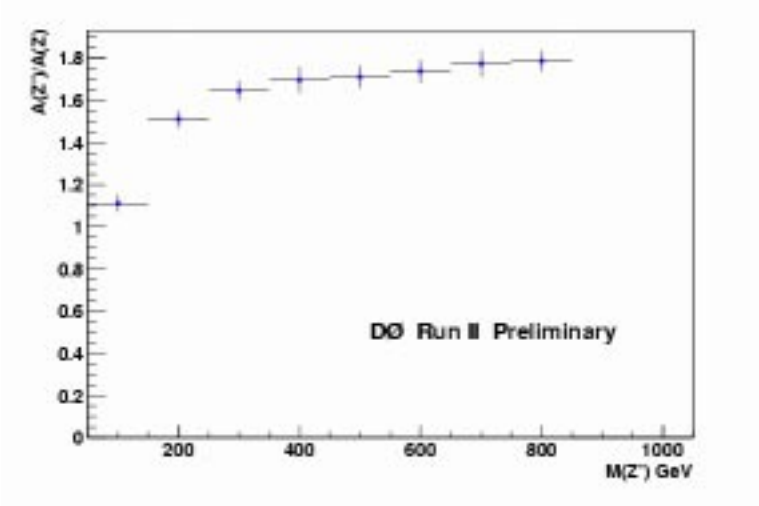

Figure 17: *Variation in acceptance as a function of the dielectron reconstructed mass.*

limit on the mass as shown in Figure 18. We obtain $M_{Z'} > 620$ GeV @ 95% c.l.

5 Summary and Conclusions

Studies at the highest mass scales in both the QCD and electroweak sectors have gotten off to a strong start at DØ in Run II. For QCD, we have observed that the dijet mass cross section agrees at all masses with NLO theory within the current errors. The inclusive jet cross section will be ready for presentation at the Summer conferences. The near-term plan involves substantially reducing the jet energy scale errors and expanding the use of the forward pseudorapidity coverage. Ultimately, we will substantially improve errors and energy resolutions through the use of tracking.

We have also augmented our existing W and Z cross section measurements in electron channels [4)] with the first Z dimuon cross section times branching ratio in Run II,

$$263.8 \pm 6.6(stat) \pm 17.3(sys) \pm 26.4(lum)\, pb.$$

The $W \to \mu\nu$ cross section, as well as updated electron analyses, will be ready for the summer conferences. A search for Z' in the dielectron channel was presented yielding a mass limit of 620 GeV at the 95% c.l.

While these results begin to approach the sensitivities of Run I, the data samples presented are just the beginning of what is expected in the coming months and years from the Tevatron. The understanding of the detector is improving rapidly, and we expect rapid progress to cutting edge science in the near future.

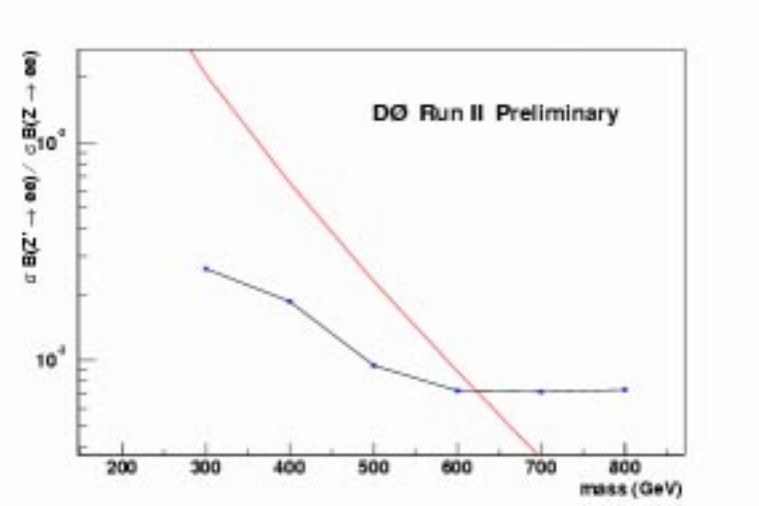

Figure 18: *Limit on cross section as a function of Z' mass (connected dots). Theoretical $\sigma * BR$ is also indicated (solid line).*

6 Acknowledgements

I would like to acknowledge the efforts of my D0 colleagues and the Tevatron staff which make these results possible. Thanks also go to the La Thuile conference organizers for a fun and enlightening meeting.

References

1. G. Blazey, et al., Proc. of Physics at Run II: QCD and Weak Boson Physics Workshop, Batavia, IL (Nov. 4-6, 1999), FERMILAB-CONF-00-092-E.

2. B. Abbott, et al., Nucl. Instr. and Meth. **A424**, 352 (1999).

3. Hamburg, van Neerven and Matsura, Nucl. Phys. **B359**, 343 (1991).

4. A. Alton (for the DØ Collab.), Proc. of 14th Topical Conf. on Hadron Collider Physics, Karlsruhe, Germany (Sep. 29-Oct. 4, 2002).